REGULAR ARTICLE

blood advances

Peripheral human red blood cell development in human immune system mouse model with heme oxygenase-1 deficiency

Aditi Khatri Patel, Kyle Trageser, Hyunjin Kim, Weikeat Lim, Christina Adler, Brace Porter, Min Ni, Yi Wei, Gurinder S. Atwal, Parnian Bigdelou, Vikas Kulshreshtha, Dharani Ajithdoss, Jun Zhong, Naxin Tu, Lynn Macdonald, Andrew Murphy, and Davor Frleta

Regeneron Pharmaceuticals, Inc, Tarrytown, NY

Key Points

- Immunodeficient mice with murine HMOX-1 deletion have persisting hRBCs in their peripheral blood.
- Immunodeficient mice with murine HMOX-1 deletion have reduced erythrophagocytic macrophages.

A challenge for human immune system (HIS) mouse models has been the lack of human red blood cell (hRBC) survival after engraftment of these immune-deficient mice with human CD34$^+$ hematopoietic stem cells (HSCs). This limits the use of HIS models for preclinical testing of targets directed at hRBC-related diseases. Although human white blood cells can develop in the peripheral blood of mice engrafted with human HSCs, peripheral hRBCs are quickly phagocytosed by murine macrophages upon egress from the bone marrow. Genetic ablation of murine myeloid cells results in severe pathology in resulting mice, rendering such an approach to increase hRBC survival in HIS mice impractical. Heme oxygenase-1 (HMOX-1)–deficient mice have reduced macrophages due to toxic buildup of intracellular heme upon engulfment of RBCs, but do not have an overall loss of myeloid cells. We took advantage of this observation and generated HMOX-1$^{-/-}$ mice on a humanized M-CSF/SIRPα/CD47 Rag2$^{-/-}$ IL-2R$_\gamma^{-/-}$ background. These mice have reduced murine macrophages but comparable levels of murine myeloid cells to HMOX-1$^{+/+}$ control mice in the same background. Injected hRBCs survive longer in HMOX-1$^{-/-}$ mice than in HMOX-1$^{+/+}$ controls. Additionally, upon human HSC engraftment, hRBCs can be observed in the peripheral blood of HMOX-1$^{-/-}$ humanized M-CSF/SIRPα/CD47 Rag2$^{-/-}$ IL-2R$_\gamma^{-/-}$ mice, and hRBC levels can be increased by treatment with human erythropoietin. Given that hRBC are present in the peripheral blood of engrafted HMOX-1$^{-/-}$ mice, these mice have the potential to be used for hematologic disease modeling, and for testing therapeutic treatments for hRBC diseases in vivo.

Introduction

Immunodeficient mouse models engrafted with a human immune system (HIS mice) represent promising platforms for preclinical testing of novel therapeutics, disease modeling, and studying basic human immunobiology. HIS mice are engrafted with human CD34$^+$ hematopoietic stem cells (HSCs) that give rise to human T cells, B cells, natural killer (NK) cells, dendritic cells, granulocytes, and myeloid cells in HIS mice.[1-4] These models have allowed testing of potential reagents directed at human leukocytes such as T-cell–activating reagents (eg, checkpoint inhibitors),[5,6] B-cell–depleting antibodies,[4,7-9] and

Submitted 21 September 2023; accepted 10 September 2024; prepublished online on *Blood Advances* First Edition 30 September 2024. https://doi.org/10.1182/bloodadvances.2023011754.

All data generated or analyzed during this study are included in this published article. The single-cell RNA sequencing data reported in this study have been deposited in the Gene Expression Omnibus (accession number GSE239736).

Any material requests should be directed to the corresponding author, Davor Frleta (Davor.Frleta@regeneron.com).

The full-text version of this article contains a data supplement.

pharmacological mobilizers of HSCs.[10-12] Additionally, HIS mice can be used for various disease modeling.[13-15]

HIS mice engrafted with HSCs do not have human red blood cells (hRBCs) present in the blood, despite developing from HSCs. Immature human reticulocytes can develop in the bone marrow (BM) of HIS mice, but they are rapidly destroyed upon egress from the BM.[16] Injection of hRBCs into nonengrafted immune–deficient mice demonstrates that hRBCs are quickly cleared from the peripheral blood, usually within hours of injection.[16] Murine macrophages are responsible for clearance of hRBCs from peripheral blood.[16-18] Treatment of HIS mice with clodronate liposomes that temporarily deplete macrophages leads to emergence of hRBCs in the peripheral blood of HIS mice and prolongs injected hRBCs in the blood.[16,17]

Prolonged removal of murine macrophages from HIS models is fraught with difficulty. Repeated injection of clodronate liposomes is not feasible because of murine toxicity. Genetic modifications that ablate murine myeloid development also negatively impact mouse development. For example, mice with a deletion of the *CSF1R* gene, the receptor for macrophage-colony stimulating factor (M-CSF) that is critical for myeloid cell development, have severe skeletal pathology and usually die before weaning.[19] This is due to a loss of osteoclasts, a subset of myeloid cells that consume bone and work in balance with osteoblasts to shape BM.[20-22] Because human HSC (hHSC) engraftment relies on hematopoiesis in the BM, HSC engraftment would be disrupted in mice lacking a BM, which would impede leukopoiesis and erythropoiesis. Thus, hRBC survival requires a HIS mouse model with a loss of murine macrophages (phagocytic cells) but not a complete loss of all murine myeloid cell subsets.

Heme oxygenase-1 (HMOX-1) is an inducible enzyme that processes heme from internalized RBCs to release and recycle iron.[23] A deficiency in human HMOX-1 was reported in a patient who died at 6 years of age.[24,25] The patient experienced growth retardation, severe anemia, and fibrosis of spleen, liver, and kidney. Because of disruption in iron recycling, iron deposition resulted in damage to the liver and kidney.[24,25] HMOX-1$^{-/-}$ mice exhibited similar pathology as the HMOX-1–deficient patient.[23,26] HMOX-1$^{-/-}$ mice develop anemia and iron overload in their kidney and liver.[20,23,26,27] They also exhibit growth retardation, and although they initially have splenomegaly, the mice develop splenic fibrosis as they age.[26,28] Because of these pathologies, HMOX-1$^{-/-}$ mice have reduced survival.[26,28]

HMOX-1$^{-/-}$ mice lack macrophages in spleen, liver, and BM because of toxic intracellular buildup of heme within macrophages that engulf RBCs.[26,27,29] Normally, phagocytosis of senescent RBCs by erythrophagocytic macrophages is necessary for clearance of dying RBCs and recycling of iron.[26,29] HMOX-1 deficiency disrupts this process, resulting in pathological iron overload in the kidney and liver.[26,27,29] Treating HMOX-1$^{-/-}$ macrophages with RBCs in vitro induces cellular death.[26] The lack of macrophages necessary for iron recycling is believed to be the primary cause of pathology in HMOX-1$^{-/-}$ given that transfer of wild-type (WT) BM ameliorates disease pathology in HMOX-1$^{-/-}$ mice.[29,30]

Despite a loss of erythrophagocytic macrophages, HMOX-1$^{-/-}$ mice still have CD11b^{+} myeloid cells.[26,27] Given the presence of CD11b^{+} myeloid cells, HMOX-1$^{-/-}$ mice do not exhibit skeletal pathology as do CSF1R$^{-/-}$ mice.[19,26,28] Furthermore, HMOX-1$^{-/-}$ mice in an immune-deficient background are healthier than their immune-competent counterparts, as noted by a lack of liver and kidney fibrosis and serum indicators of liver and kidney health. The loss of macrophages that engulf RBCs, without the concomitant loss of all myeloid cell subsets, makes HMOX-1 deficiency a promising approach to support hRBC development in hHSC-engrafted HIS mice.

Herein we demonstrate that deleting HMOX-1 in our immune-deficient mice (hSIRPα/hM-CSF/hCD47/Rag2$^{-/-}$/IL-2Rγ$^{-/-}$ HIS mice) allowed for the survival of hRBCs with either passively injected hRBCs or hHSC engraftment of the mice.

Methods

Mice

For the generation of HMOX-1$^{-/-}$ mice, the mouse *Hmox1* gene was knocked out in the mouse genome using VelociGene technology (Regeneron Pharmaceuticals). An ~7-kb mouse genomic sequence of the Hmox1 gene, from the start codon ATG to the stop codon, was deleted on mouse chromosome 8 C1, between chromosome 8 (chr8) coordinates 75093750 and 75100019 (Genome Reference Consortium Mouse Build 38 [GRCm38] assembly). To create the targeting vector from mouse bacterial artificial chromosome clone RP23-102I24 by the bacterial homologous recombination step, a hygromycin (Hyg) resistance self-deletion cassette (with Cre recombinase controlled by the protamine promoter) flanked by lox sites (lox2372-hyg-lox2372) was used to replace the ~7-kb mouse sequence containing the mouse *Hmox1* gene. Mouse homology arms were made by polymerase chain reaction amplification using bacterial artificial chromosome clone RP23-102I24 as the template: the 5′ homology arm with 5′ primer GATGTTGCAACAGCAGCGAGAA and 3′ primer CACCGGACTGGGCTAGTTCA; and the 3′ homology arm by 5′ primer ATGCAATACTGGCCCCCAGG and 3′ primer GAT TTGGGGCTGCTGGTTTCAA.

The final targeting vector contained, from 5′ to 3′, the chloramphenicol resistance cassette, the 5′ mouse homology arm, the lox2372-Hyg-lox2372 self-deletion cassette, and the 3′ mouse homology arm. The final clone was selected on the basis of chloramphenicol and Hyg resistance, and the targeting vector was electroporated into mouse embryonic stem (ES) cells with humanized SIRPα, humanized M-CSF, humanized CD47, and Rag2$^{-/-}$ IL-2Rγ$^{-/-}$. Targeted homologous recombination resulted in deletion of ~7 kb of mouse sequence (GRCm38 coordinates chr8: 75093750-75100019). Successful integration was confirmed by a modification of allele (MOA) assay. Primers and probes used for the MOA assay to detect the loss of mouse *Hmox1* sequences included the Hmox1_U Probe (TCAGACGATTTGTAAGATGCAGGGA) and Hmox1_D Probe (TGTAGCAGATCCT GGCCTTGGAC).

The mouse embryo comprising the donor ES cells was incubated in vitro and then implanted into a surrogate mother to produce an F0 mouse fully derived from the donor ES cells. Mice with deleted *Hmox1* gene were identified by genotyping using the MOA assay described above. Mice heterozygous for the knockout *Hmox1* gene were bred to homozygosity. Mice were maintained on a sulfa diet (LabDiet, St. Louis, MO) in an pathogen free facility, and were interbred for ~5 to 10 generations. All experiments were

conducted in compliance with the Regeneron Institutional Animal Care and Use Committee protocols. Human fetal liver (FL) samples used for isolating human $CD34^+$ HSCs were obtained from Advanced Biosciences Resources (Alameda, CA) with appropriate informed consent.

Passive transfusion of hRBCs

In nonengrafted HMOX-$1^{+/+}$ and HMOX-$1^{-/-}$ hSIRPα/hM-CSF/hCD47/$Rag2^{-/-}$/IL-$2R\gamma^{-/-}$ mice, 4×10^7 hRBCs were injected intraperitoneally (n = 7 per mouse strain). Mice were bled daily until day 8 after injection, and blood was collected in phosphate-buffered saline (PBS) + 5-mM EDTA for counting and fluorescence-activated cell sorting analysis.

Human $CD34^+$ cell isolation

Human FL samples were obtained from Advanced Biosciences Resources with appropriate informed consent. FL samples were cut in small fragments and treated for 25 minutes at 37°C with Collagenase D (100 ng/mL; Roche). The cell suspension was prepared, and the human $CD34^+$ cells were separated by density-gradient centrifugation, followed by positive immunomagnetic selection using anti-human CD34 microbeads according to the manufacturer's instructions (Miltenyi Biotec). Cells were either frozen in 10% dimethyl sulfoxide containing human albumin serum and kept in liquid nitrogen or injected directly.

Human $CD34^+$ immune cell reconstitution

Newborn pups were sublethally irradiated (160 cGy; Rad2000 irradiator (RAD Source Technologies, Inc) 4 to 24 hours before intrahepatic injection of 1×10^5 human FL–derived $CD34^+$ cells.

Analysis of human hematopoietic cell populations

For analyzing hRBC populations, blood was collected in PBS + 5-mM EDTA and counted using a Beckman Coulter counter. Whole blood cells were stained with the following monoclonal antibodies for flow cytometry analysis: phycoerythrin (PE) anti-human CD235a (clone HI264; BioLegend) and PE/Cyanine7 anti-mouse TER-119 (clone: TER-119; BioLegend). For overall hematopoietic engraftment, blood was collected retro-orbitally 10 to 12 weeks after engraftment. RBCs were lysed using ACK (ammonium-chloride-potassium) (Gibco, Thermo Fisher Scientific), and the cells were stained with the following monoclonal antibodies for flow cytometry analysis: BD Pharmingen APC-Cy7 Rat Anti-Mouse CD45 (clone: 30-F11; BD Biosciences), anti-human CD45 Monoclonal Antibody, PE-Cyanine5.5 (clone: HI30; Invitrogen, Thermo Fisher Scientific), FITC Mouse Anti-Human CD19 (clone: HIB19; BD Biosciences), anti-human CD3 Monoclonal Antibody, Pacific Blue (clone: S4.1; Invitrogen), BD Pharmingen APC Mouse Anti-Human CD335 (NKp46) (clone: 9E2; BD Biosciences), and PE/Cyanine7 anti-human CD14 Antibody (clone: M5E2; BioLegend). The samples were acquired by LSRFortessa (BD Biosciences) or FACSymphony (BD Biosciences) and analyzed using FACSDiva (BD Biosciences) and FlowJo software (FlowJo LLC). Mice with ≥10% human $CD45^+$ of total circulating $CD45^+$ cells (total including both mouse and human $CD45^+$ cells) were used for experiments. For experimental repeats, different donor sources of human $CD34^+$ cells were used. Donor-to-donor variations in human $CD45^+$ levels (human leukocytes) were comparable to the range of variation observed between individual mice engrafted with $CD34^+$ cells from the same donor.

Analysis of murine monocytes and macrophages

For analysis of mouse myeloid cells, single-cell suspensions were prepared from spleen and liver and mechanically digested followed by passage through a 70-μM filter. RBCs were lysed using ACK (Gibco), and the cells were stained with the following monoclonal antibodies for flow cytometry analysis: BD Pharmingen APC-Cy7 Rat Anti-Mouse CD45 (clone: 30-F11; BD Biosciences), anti-human CD45 Monoclonal Antibody, PE-Cyanine5.5 (clone: HI30; Invitrogen), Brilliant Violet 605 anti-mouse/human CD11b Antibody (clone M1/70; BioLegend), BD Pharmingen Purified Rat Anti-Mouse CD14 (clone: rmC5-3; BD Biosciences), BD Pharmingen PE Rat Anti-Mouse CD106 (clone: 429; BD Biosciences), PE/Dazzle 594 anti-mouse F4/80 Antibody (clone: BM8; BioLegend), PE/Cyanine7 anti-human CD14 Antibody (clone: M5E2; BioLegend), anti-human CD206 Brilliant Violet 785 (clone: 15-2; BioLegend), and Alexa Fluor 700 anti-human CD36 Antibody (clone: 5-271; BioLegend). The samples were acquired by LSRFortessa or FACSymphony, and analyzed using FACSDiva and FlowJo software.

hEPO treatment

hHSC-engrafted HMOX-$1^{-/-}$ hSIRPα/hM-CSF/hCD47/$Rag2^{-/-}$/IL-$2R\gamma^{-/-}$ mice were retro-orbitally bled to analyze preinjection levels of hRBCs and then injected with 100 units of human erythropoietin (hEPO) (R&D systems) intraperitoneally. One week later, mice were again retro-orbitally bled to check hRBC and total RBC levels.

Serum chemistry and heme analysis

Blood was acquired from mice via cardiac puncture and collected using serum separator tubes. Serum was used for analysis of liver enzymes, including aspartate aminotransferase (AST), alanine transaminase (ALT), and alkaline phosphatase (ALP), as well as creatinine, which is an indicator of kidney function. AST, ALT, ALP, and creatinine were analyzed using the Advia Chemistry XPT System (Siemens).

Total human immunoglobulin M (IgM) and IgG were analyzed from serum through a standard sandwich enzyme-linked immunosorbent assay. Briefly, 96-well clear-bottom slides (Nunc, Thermo Fisher Scientific) were coated with anti-human IgM or anti-human IgG capture antibodies (Jackson ImmunoResearch). The plate was then blocked with PBS-Tween 20% and 5% bovine serum albumin. Diluted serum samples (HIS and normal human serum) were added along with human IgM and IgG standards (Jackson ImmunoResearch). The plates were washed with PBS-Tween 20, and anti-human IgM and IgG detection antibodies conjugated to horseradish peroxidase were added. After incubation, the plates were washed again, and OptEIA TMB substrate (Invitrogen) was added for development. The reaction was stopped with 1N sulfuric acid, and IgM and IgG levels were visualized using an enzyme-linked immunosorbent assay reader (Molecular Devices).

Serum was also analyzed for heme levels. Spleen heme levels were analyzed by mechanical digestion of spleens in PBS, followed by passage through a 70μM filter. The single-cell suspension was centrifuged at >500*g* for 5 minutes and supernatant collected for

heme analysis. Heme levels from serum and splenic supernatant were analyzed using a Heme Assay Kit (MilliporeSigma) according to manufacturer instructions. Splenic heme levels were normalized to spleen size, and the spleens showed no morphological differences other than size.

Tissue analysis

Liver and kidney tissues were harvested from WT, nonengrafted HMOX-1$^{+/+}$, nonengrafted HMOX-1$^{-/-}$, engrafted HMOX-1$^{+/+}$, and engrafted HMOX-1$^{-/-}$ mice. Tissues were fixed in 10% formalin for 24 hours and then transferred into 70% ethanol for 48 hours. The tissues were processed in a Leica tissue processor and paraffin-embedded. Sections of 5-μM thickness were baked onto slides, and slides were deparaffinized and rehydrated for staining. Kidney sections were stained with a Masson Trichrome Stain Kit (StatLab) according to the manufacturer's protocol. Liver and kidney sections were stained with a Prussian Blue kit (Polysciences, Inc) according to the manufacturer's protocol. Liver sections were stained in Mayer's hematoxylin for 1 minute and washed with tap water. The nuclei were blued in 1× PBS for 1 minute and washed three 3 in distilled water. The sections were counterstained in alcoholic eosin for 1 minute and then dehydrated. The slides were cleared in xylene and coversliped. Scanned whole-slide images were evaluated by board-certified veterinary pathologists. Fibrosis was scored on Masson's trichome–stained sections using a semiquantitative grading scale: 0, within normal limits; 1, minimal; 2, mild; 3, moderate; and 4, severe. Iron accumulation was scored on Prussian blue–stained sections using a semiquantitative grading scale: 0, within normal limits; 1, rare (<1% stained cells); 2, minimal (1%-10% stained cells); 3, mild (10%-30% stained cells); 4, moderate (30%-60% stained cells); and 5, severe (60%-100% stained cells).

Single-cell RNA sequencing (RNAseq) analysis

Mouse and human CD45^{+} cell fractions were collected from the spleens of hHSC-engrafted HMOX-1$^{+/+}$ and HMOX-1$^{-/-}$ hSIRPα/hM-CSF/hCD47/Rag2$^{-/-}$/IL-2Rγ$^{-/-}$ mice. Cells were isolated by positive magnetic enrichment using either mouse CD45 or human CD45 microbeads (Miltenyi Biotec). Isolated cells were processed using the 10× 5′NextGEM v2 library kit. After the processing, Cell Ranger, version 6.1.1 (10x Genomics) with the GRCh38 reference was used on the processed cells to compute gene expression levels and to generate analysis-ready data. We checked the quality of the data (number of cells, mean reads per cell, median genes per cell, median unique molecular identifier counts per cell, etc.) to filter out artifacts, empty droplets, and multiplets. In each sample, cells with a total number of molecules detected within a cell >30 000 and <1000 were filtered out. Then, the Python module Scanpy (version 1.7.1) was used to normalize the data. The normalization was performed as follows: (1) transformation of total counts so that each cell sums to 10 000, (2) log1p transformation of the counts, and (3) unit scaling of the gene expression counts across all cells to ensure a mean of 0 and a maximum value of 10. Lastly, R Seurat package (version 4.3.0.1) was used to generate uniform manifold approximation and projection plots and to run clustering. In each cluster, we identified markers based on differentially expressed genes, and cell types were assigned to the clusters on the basis of the top markers. Cell type percentages were calculated as (the number of cells for the cell type × 100/the total number of cells in the condition).

Statistical analysis

Statistical analysis was performed using GraphPad Prism (version 9.4.1; GraphPad Software, San Diego, CA). Statistical significance was evaluated in most figures using an unpaired Student *t* test. Statistical significance of hEPO treatment was evaluated by paired Student *t* test.

Results

A 7-kb mouse genomic sequence of the *Hmox1* gene, from the start codon ATG to the stop codon, was deleted on mouse chromosome 8 C1, between coordinates chr8 75093750 and 75100019 (GRCm38 assembly) to create the targeting vector, which was electroporated into mouse ES cells with humanized SIRPα, humanized M-CSF, humanized CD47, and Rag2$^{-/-}$ IL-2Rγ$^{-/-}$ (Figure 1). F0 mice were bred to homozygosity for all alleles.

HMOX-1$^{-/-}$ and HMOX-1$^{+/+}$ mice in the hSIRPα/hM-CSF/hCD47/Rag2$^{-/-}$/IL-2Rγ$^{-/-}$ background were injected intraperitoneally with hRBCs. At day 1 after injection, no hRBCs could be detected in the peripheral blood of HMOX-1$^{+/+}$ mice (Figure 2A). In contrast, injected hRBCs survived for >1 week in the peripheral blood of HMOX-1$^{-/-}$ (Figure 2A). Notably, the level of total RBCs (mouse and human) was not different between HMOX-1$^{-/-}$ and HMOX-1$^{+/+}$ mice (Figure 2B).

HMOX-1$^{-/-}$ and HMOX-1$^{+/+}$ mice were engrafted with hHSCs, and the development of a HIS was analyzed in these mice. At 12 weeks after engraftment, human CD45^{+} levels were slightly higher in HMOX-1$^{-/-}$ mice, although BM engraftment was comparable between HMOX-1$^{+/+}$ and HMOX-1$^{-/-}$ HIS mice (Figure 3A). Notably, downregulation of HMOX-1 has been described to increase engraftment with murine HSCs.[31] Because HIS mice were engrafted with only 100 000 HSCs, the frequency of hematopoietic stem and progenitor cells in the BM is generally too low for appreciable quantification. Nonetheless, the level of HIS engraftment is substantial. With HIS engraftment, total RBCs were significantly reduced ($P < .0001$) in both HMOX-1$^{+/+}$ and HMOX-1$^{-/-}$ HIS mice (Figure 3B). This has previously been described in HIS models with humanized M-CSF due to the increased human macrophages phagocytosing murine RBCs.[2] HMOX-1$^{-/-}$ HIS mice had lower levels of human B cells and greater levels of human myeloid cells in blood and BM compared with HMOX-1$^{+/+}$ HIS mice (Figure 3C-D). HMOX-1$^{-/-}$ HIS mice had greater levels of human NK cells in the BM compared with HMOX-1$^{+/+}$ HIS mice (Figure 3D). Despite lower human B-cell levels in HMOX-1$^{-/-}$ HIS mice, there was significantly higher human IgG in the serum of HSC-engrafted HMOX-1$^{-/-}$ mice than in HMOX-1$^{+/+}$ HIS mice, with similar levels of serum human IgM (supplemental Figure 1). Although both HMOX-1$^{-/-}$ and HMOX-1$^{+/+}$ HIS mice had lower levels of IgM/IgG than those found in normal human serum (supplemental Figure 1), this is common in HIS mice because of dysfunctional human B-cell responses.[3]

In contrast to HSC donor-matched HMOX-1$^{+/+}$ mice, hHSC-engrafted HMOX-1$^{-/-}$ mice had hRBCs in peripheral blood (Figure 3E). In the BM, both hHSC-engrafted HMOX-1$^{+/+}$ and HMOX-1$^{-/-}$ mice had hRBCs, with higher levels in HMOX-1$^{-/-}$ HIS mice (Figure 3F). This indicated that although hRBCs can develop in the BM of HIS mice, HMOX-1$^{-/-}$ HIS mice allow hRBCs to survive in the peripheral blood.

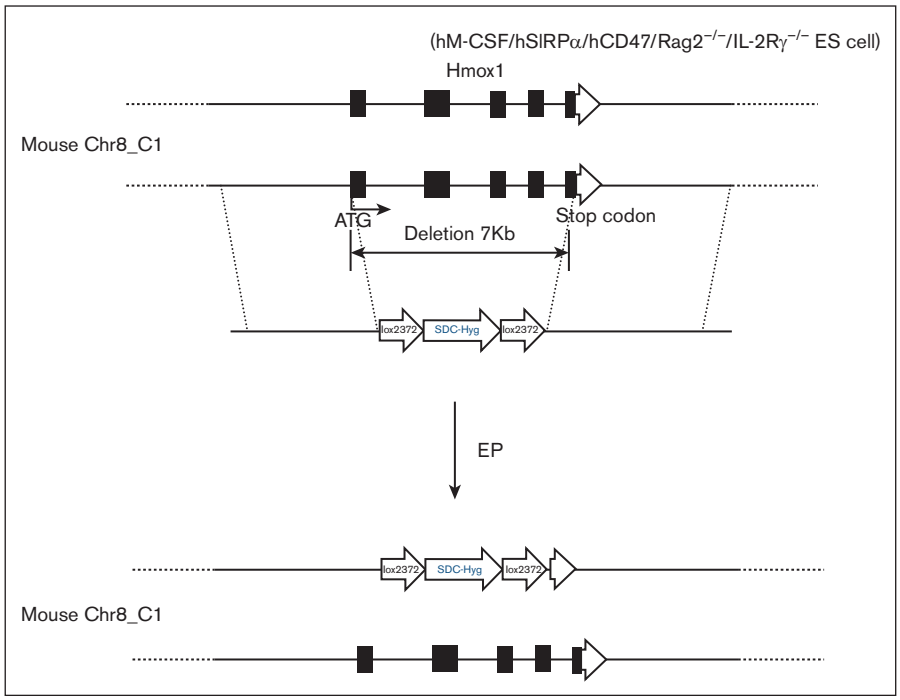

Figure 1. HMOX-1 KO design. A 7-kb mouse genomic sequence of the mouse *Hmox-1* gene, from the start codon ATG to the stop codon, was deleted on mouse chromosome 8 C1, between coordinates chr8 75093750 and 75100019. The deletion was performed in ES cells with humanized M-CSF, SIRPα, CD47, and deletion of mouse Rag2 and IL-2Rγ genes. The mouse embryo comprising the donor ES cells was incubated in vitro and then implanted into a surrogate mother to produce an F0 mouse fully derived from the donor ES cells. Mice with Hmox-1 gene deleted were identified by genotyping using the MOA assay described above. Mice heterozygous for deletion of the Hmox-1 gene were bred to homozygosity for all genes. EP, electroporation; KO, knockout.

Erythropoietin (EPO) increases RBC output from the BM.[32,33] Injection of human EPO into hHSC-engrafted HMOX-1$^{-/-}$ mice increased the percentage (Figure 4A) and number (Figure 4B) of hRBCs in the peripheral blood. However, there was no effect on total RBC numbers (Figure 4C) since most RBCs in the HMOX-1$^{-/-}$ HIS mice are murine, and hEPO does not cross-react with murine erythropoietin receptor (EpoR).[34]

We analyzed macrophage levels in spleen and liver of HMOX-1$^{-/-}$ and HMOX-1$^{+/+}$ controls. No significant differences were noted in mouse CD11b^{+}/CD14^{+} monocytes between HMOX-1$^{-/-}$ and HMOX-1$^{+/+}$ spleen. However, HMOX-1$^{-/-}$ had a reduction in F4/80^{+}/vascular cell adhesion molecule^{+} macrophage subset relative to HMOX-1$^{+/+}$ spleen (Figure 5A). The liver is considered a major site of hRBC clearance in mice.[13] Accordingly, we observed a reduction of murine F4/80^{+} macrophages in the liver of HMOX-1$^{-/-}$ mice relative to HMOX-1$^{+/+}$ mice, along with a concomitant increase in overall murine CD11b^{+} monocytes in HMOX-1$^{-/-}$ mice (Figure 5B). As shown in Figure 3B, there was an increase in human myeloid cells in the blood of HMOX-1$^{-/-}$ HIS mice. There was also a slight increase in human monocytes (denoted as hCD14^{+}) in the spleen and liver of HMOX-1$^{-/-}$ HIS mice (Figure 5C). Furthermore, analysis of hCD36^{+}/CD206^{+} human macrophage populations indicated an increase in this specific

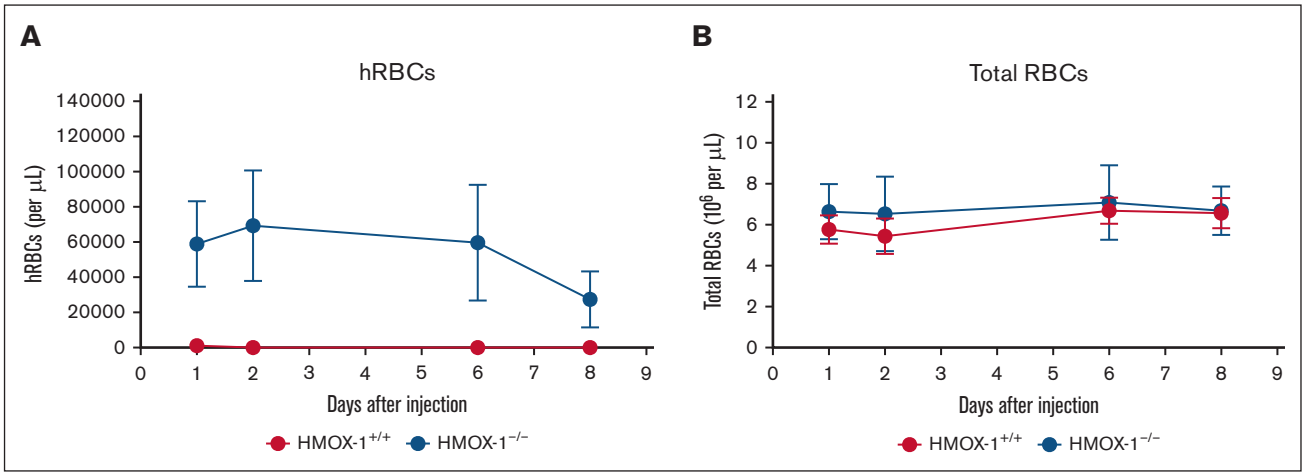

Figure 2. Injected hRBCs survive longer in HMOX-1$^{-/-}$ mice than in HMOX-1$^{+/+}$ mice. Human RBCs were injected intraperitoneally into nonengrafted HMOX-1$^{+/+}$ (n = 7) and HMOX-1$^{-/-}$ MSRG47 mice (n = 7). Mice were bled retro-orbitally at days 1, 2, 6, and 8 after injection and analyzed for human RBCs (hCD235a^{+}) vs mouse RBCs (Ter-119^{+}). (A) Number of hRBCs per microliter of blood. (B) Total RBCs (human and mouse) per microliter of blood.

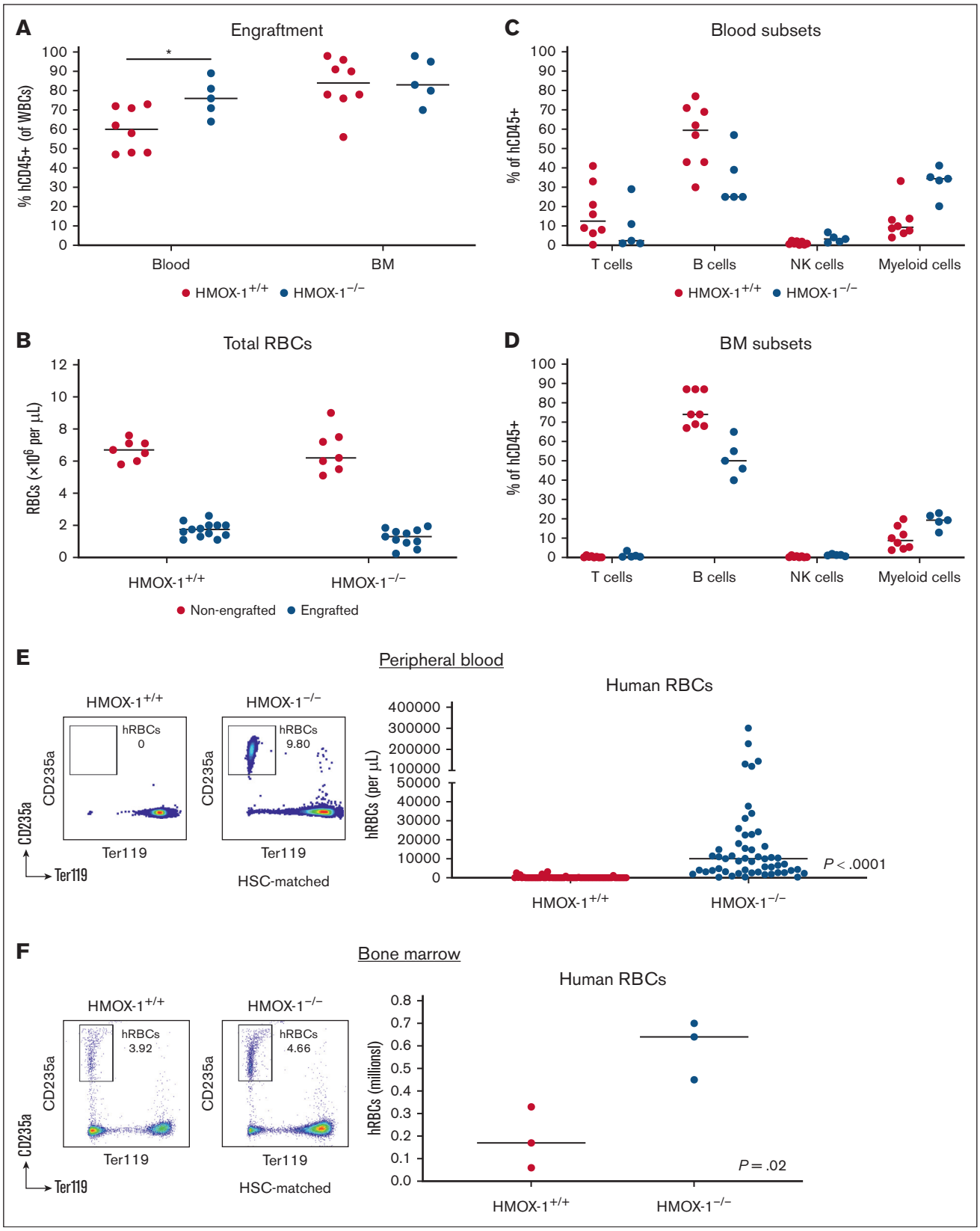

Figure 3. HMOX-1$^{-/-}$ HIS mice have hRBCs in peripheral blood. HMOX-1$^{-/-}$ and HMOX-1$^{+/+}$ MSRG47 mice were intrahepatically engrafted with hHSCs. At 12 weeks after engraftment, mice were examined for (A) total circulating hCD45^{+} cells (human leukocytes) in the peripheral blood and BM. (B) Total RBC levels in the blood of nonengrafted vs engrafted HMOX-1$^{+/+}$ and HMOX-1$^{-/-}$ mice. (C) Levels of human CD3^{+} T cells, CD19^{+} B cells, NKp46^{+} NK cells, and CD14^{+} myeloid cells (as percentage of total hCD45^{+} cells)

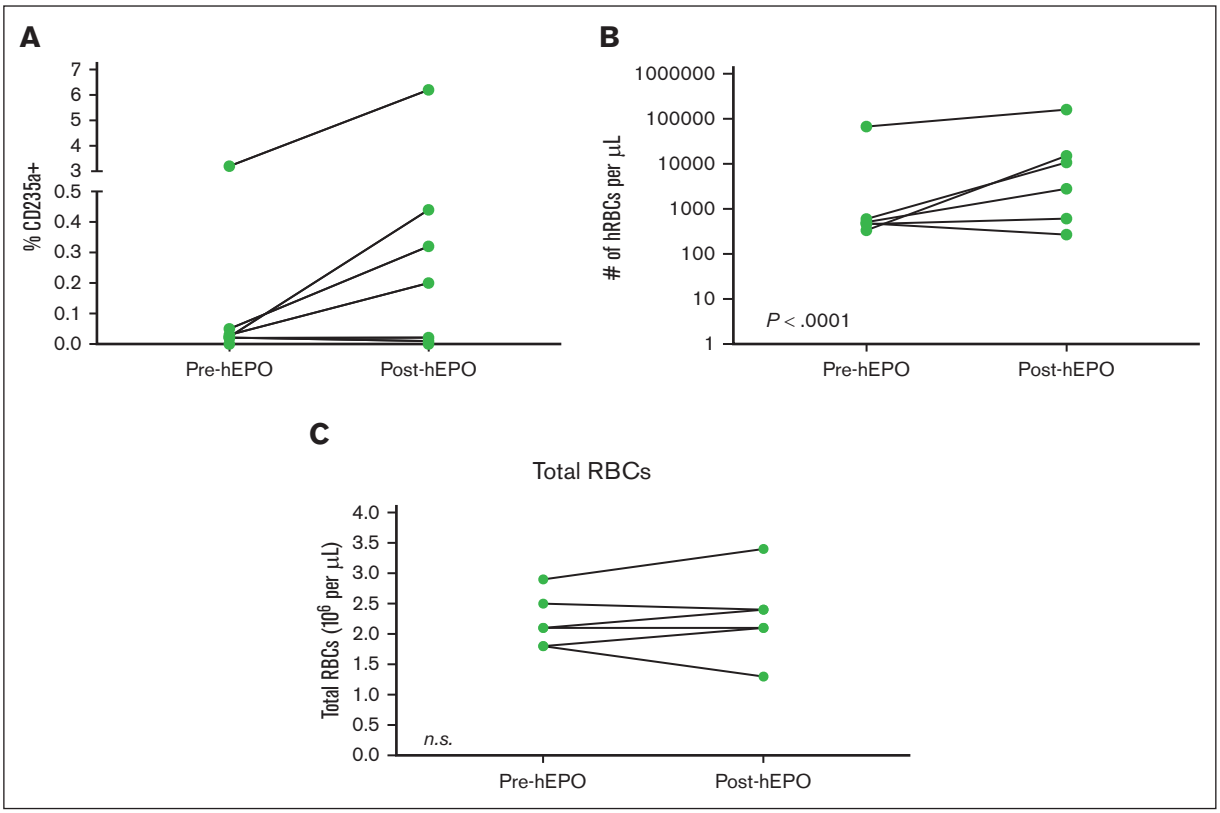

Figure 4. Human EPO increases hRBC levels in peripheral blood of HMOX-1$^{-/-}$ HIS mice. HMOX-1$^{-/-}$ MSRG47 mice were intrahepatically engrafted with hHSCs. At 12 weeks after engraftment, mice were bled retro-orbitally to examine the level of hRBCs in peripheral blood before being injected intraperitoneally with 100 units of hEPO. At 1 week after injection, hRBCs were reassessed from the retro-orbital bleed. (A) Percentage of hRBCs in peripheral blood of HMOX-1$^{-/-}$ MSRG47 mice before and after hEPO treatment. (B) Total number of hRBCs per microliter of peripheral blood before and after hEPO treatment. (C) Total number of RBCs per microliter of peripheral blood before and after hEPO treatment. Two independent experiments were performed. Data represent the mean ± SEM with individual mice shown. Statistical analysis was evaluated by paired Student *t* test.

human macrophage population in the spleen (Figure 5C). This population was also increased in the liver of HMOX-1$^{-/-}$ HIS mice (Figure 5C).

Flow cytometric analysis showed a reduction in murine macrophages without a loss of overall murine monocytes in HMOX-1$^{-/-}$ mice (Figure 5). We further wanted to determine if there are differences in human leukocytes that develop from hHSC engraftment of HMOX-1$^{+/+}$ vs HMOX-1$^{-/-}$ HIS mice. Thus, single-cell RNAseq was performed on mouse and human CD45^{+} leukocytes isolated from the spleen of HMOX-1$^{+/+}$ and HMOX-1$^{-/-}$ mice. We first show the various subsets of murine CD45^{+} leukocytes in the spleen of engrafted MSRG47 mice (Figure 6A). Murine macrophages are selectively diminished in the spleen of HMOX-1$^{-/-}$ mice, and these macrophages are denoted "erythroblastic" (EB) macrophages because they share genes that are commonly found on erythrocytes, such as *EpoR*, *KLF1*, and hemoglobin-associated genes *Hbb* and *Hba*. This subset of macrophages is involved in the formation of EB islands for RBC maturation and erythrophagocytosis of senescent RBCs.[35-38] Remarkably, single-cell RNAseq analysis of human CD45^{+} cells in the spleen indicated a loss of human EB macrophages and a significant reduction in human B cells (Figure 6B). Whereas human EB macrophages were reduced in the spleen of HMOX-1$^{-/-}$ mice, there was still an increase in overall human macrophages, confirming what was previously shown by fluorescence-activated cell sorting analysis (Figure 5C).

Human macrophages may have ameliorated certain pathologies exhibited by HMOX-1$^{-/-}$ mice. Elevated heme levels have been described in HMOX-1–deficient mice, and whereas heme was elevated in both the serum and spleen of nonengrafted HMOX-1$^{-/-}$

Figure 3 (continued) are shown in the blood. (D) Levels of human CD3^{+} T cells, CD19^{+} B cells, NKp46^{+} NK cells, and CD14^{+} myeloid cells (as percentage of total hCD45^{+} cells) are shown in the BM. HMOX-1$^{+/+}$ compared with HMOX-1$^{-/-}$: T cells, no significant difference; blood B cells, $P = .006$; BM B cells, $P = .0005$; blood NK cells, no significant difference; BM NK cells, $P = .0059$; blood myeloid cells, $P = .03$; and BM myeloid cells, $P = .01$. (E) Number of hRBCs per microliter of blood of HMOX-1$^{+/+}$ and HSC donor-matched HMOX-1$^{-/-}$ HIS mice. At least 7 independent experiments were performed. (F) Total number of hRBCs in the BM of HMOX-1$^{+/+}$ and HSC donor-matched HMOX-1$^{-/-}$ HIS mice is shown. Data represent the mean ± standard error of the mean (SEM) with individual mice shown. Statistical analysis was evaluated by unpaired Student *t* test. Experimental analysis was performed at least 3 times, with representative analysis shown.

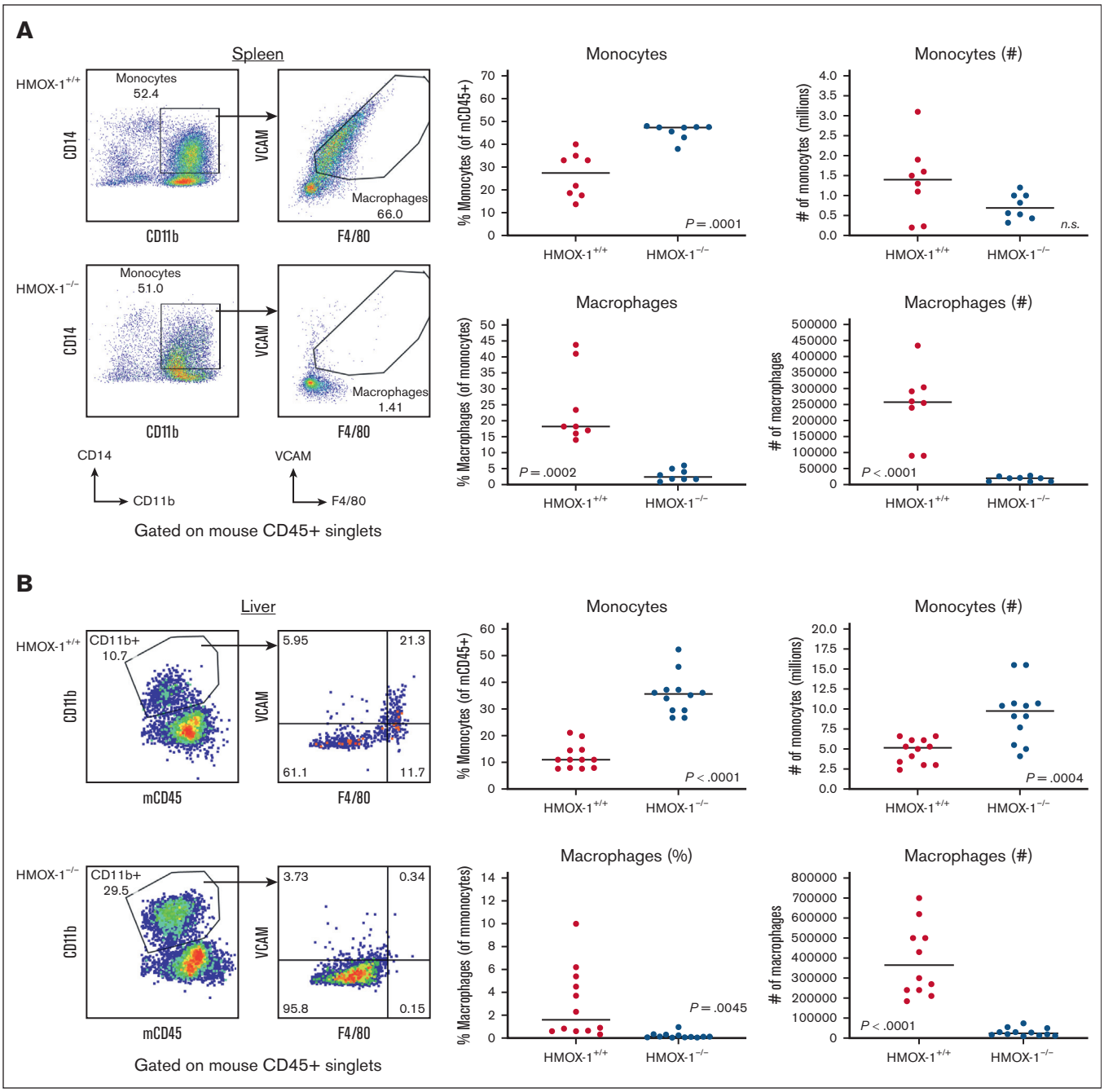

Figure 5. HMOX-1$^{-/-}$ HIS mice have reduced murine macrophages but no decrease in monocytes. HMOX-1$^{-/-}$ and HMOX-1$^{+/+}$ MSRG47 mice were hHSC engrafted. At 12 weeks after engraftment, spleen and liver tissues were harvested for single-cell preparation. Mouse monocytes and macrophages were analyzed in spleen by examining mouse CD45^{+} leukocytes for CD11b^{+}/CD14^{+} (monocytes), with macrophages denoted as mouse VCAM^{+}/mouse F4/80^{+} cells (A). (B) For liver analysis, mouse CD45^{+} leukocytes were analyzed for CD11b^{+} cells (monocytes) and macrophages denoted as a subset of CD11b^{+} cells that are mouse VCAM^{+}/mouse F4/80^{+}. (C) Human monocytes and macrophages were analyzed in spleen and liver by examining human CD45^{+} leukocytes for CD14^{+} (monocytes) with CD36^{+}/CD206^{+} macrophages examined as a subpopulation of human CD14^{+} cells in spleen and liver. At least 3 independent experiments were performed. Data represent the mean ± standard error of the mean, with individual mice shown. Statistical analysis was evaluated by unpaired Student *t* test. VCAM, vascular cell adhesion molecule.

mice, HIS engraftment greatly reduced both serum (supplemental Figure 2A) and spleen heme (supplemental Figure 2B) in HMOX-1$^{-/-}$ mice. No morphological difference between spleens other than size was observed. Engrafted mice had larger spleens due to more immune cells. Furthermore, iron deposition in the kidneys of HMOX-1$^{-/-}$ mice was decreased upon HIS engraftment (supplemental Figure 3A). No iron accumulation was observed in other groups. Minimal fibrosis was observed in the interstitium in all

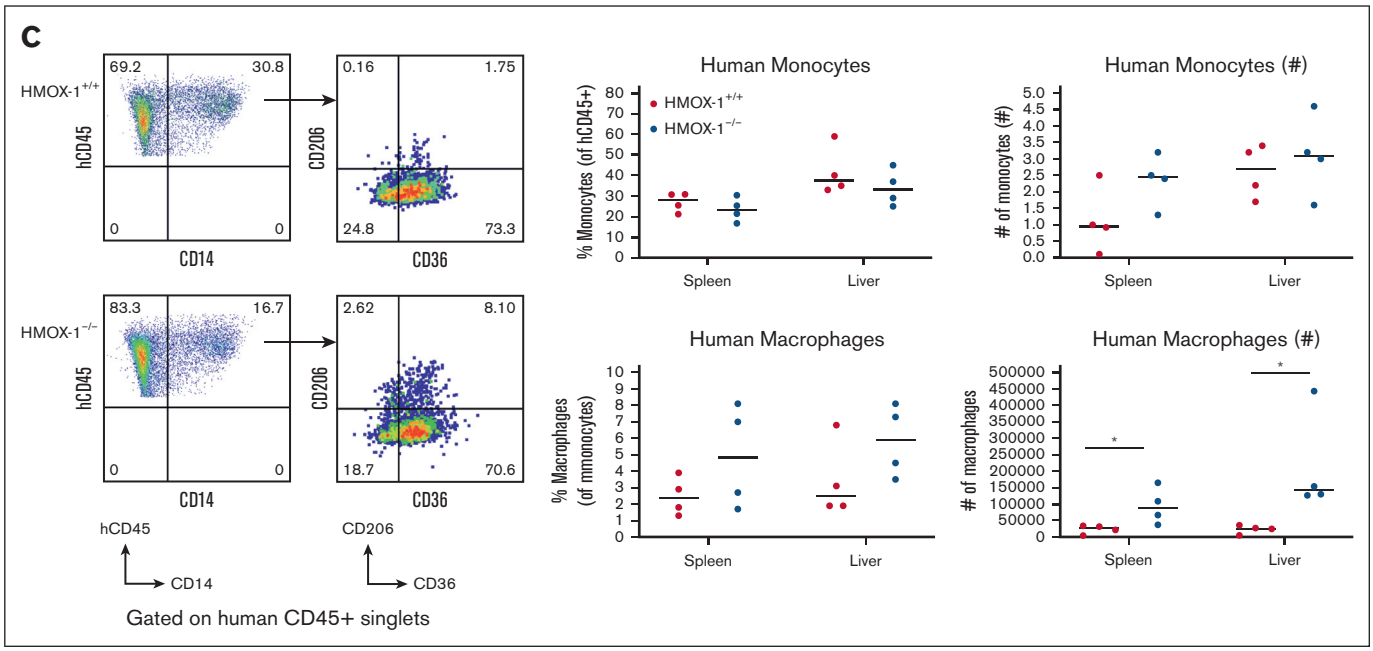

Figure 5 (continued)

groups (supplemental Figure 3B). In contrast, the liver of engrafted HMOX-1$^{-/-}$ mice exhibited the highest amount of iron accumulation in the hepatocytes and Kupffer cells, followed by engrafted HMOX-1$^{+/+}$ mice (supplemental Figure 3C). No or rare iron accumulation was observed in other groups. There was no evidence of fibrosis within the examined sections (supplemental Figure 3D).

Levels of liver enzymes including AST and ALT were similar between HMOX-1$^{+/+}$ and HMOX-1$^{-/-}$ mice, whether engrafted or nonengrafted (supplemental Figure 4A). Engraftment led to an increase in ALP, but there was no significant difference between HMOX-1$^{+/+}$ and HMOX-1$^{-/-}$ HIS mice (supplemental Figure 4A). Furthermore, creatinine, an indicator of kidney pathology, was normal in both HMOX-1$^{+/+}$ and HMOX-1$^{-/-}$ mice (engrafted and nonengrafted) (supplemental Figure 4B), further supporting histology data on the lack of kidney pathology (supplemental Figure 3B).

Discussion

Herein we demonstrated that HMOX-1 deficiency in a humanized M-CSF/SIRPα/CD47 and Rag2$^{-/-}$/IL-2R$_{\gamma}^{-/-}$ background allows for the presence of peripheral blood hRBCs, generated from hHSC engraftment or injection of hRBCs into nonengrafted mice. The survival of hRBCs in mice is dependent on the removal of specific murine macrophage subsets. Unlike other approaches that use clodronate liposomes to remove phagocytic macrophages, HMOX-1 deletion is a genetic approach that renders the mouse environment permissive to hRBCs and does not require further manipulations. Additionally, unlike genetic deletions that ablate all murine myeloid cells, which have deleterious effects on mouse development,[19] HMOX-1 deletion leads to the loss of specific murine macrophage subsets that are most associated with erythrophagocytosis, as revealed by single-cell RNAseq analysis. This leads to a HIS model that permits the study of hRBCs in mice.

Recently, Song et al[13] used a genetic approach to delete fumarylacetoacetate hydrolase (FAH) in immunodeficient MISTRG mice. FAH deletion in hHSC-engrafted MISTRG mice allows for the ablation of murine liver cells and replacement with human liver cells.[13] Song et al[13] demonstrated that hRBCs in these mice are cleared in the liver by murine Kupffer cells, a tissue-specific macrophage subset, and by ablating murine liver cells there is a decrease in murine Kupffer cells that allows for hRBC survival. Despite the MISTRG-FAH model representing a breakthrough for hRBC survival in HIS mice, it still requires further manipulation. Murine hepatocytes must be eliminated and concurrently replaced with human hepatocytes, but this requires (1) surgical implantation of human hepatocytes, and (2) at least 4 weeks of cycling the mice on/off nitisinone water to achieve replacement with human liver.[13,17] With HMOX-1 deficiency in an immune-deficient mouse model, additional manipulation is unnecessary for hRBCs because of the genetic deletion of HMOX-1 eliciting a steady-state loss of specific murine macrophages. As demonstrated, hRBCs survive longer in the peripheral blood upon passive transfusion of human blood or can develop via erythropoiesis from hHSC engraftment.

Song et al[13] speculated that the humanized M-CSF in the MISTRG-FAH model further diminishes re-establishment of murine Kupffer cells in the murine liver upon liver humanization by skewing the balance between mouse and human myeloid cells. We believe that this did not occur in our HMOX-1$^{-/-}$ HIS model because the ablation of murine macrophages occurs at steady state without any further intervention. Furthermore, loss of murine macrophages in this model is not dependent on hHSC engraftment.

The HMOX-1$^{-/-}$ HIS mouse model reported herein includes humanization of the M-CSF cytokine, which increases human myeloid/macrophage levels upon hHSC engraftment, similarly to

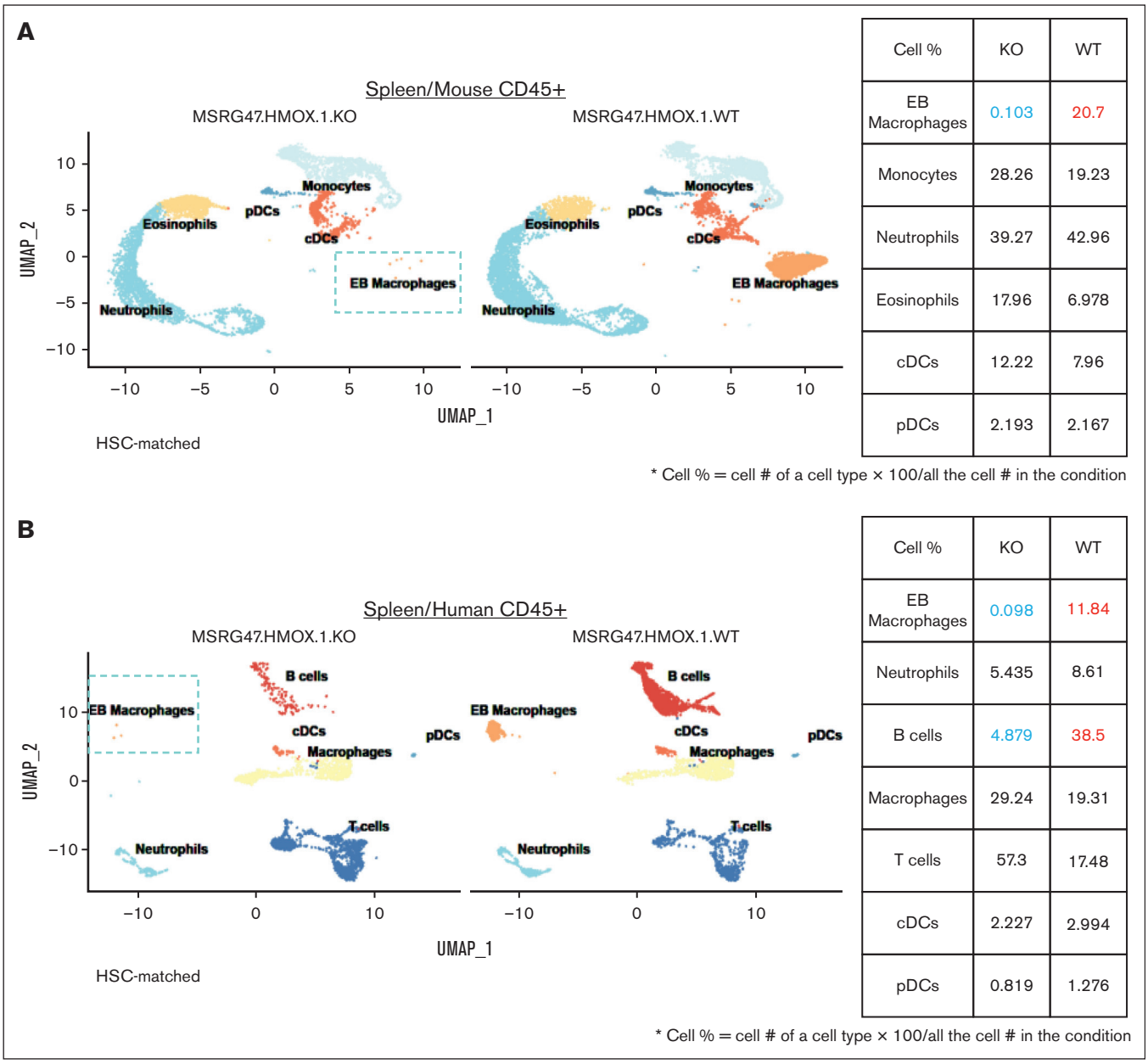

Cell %	KO	WT
EB Macrophages	0.103	20.7
Monocytes	28.26	19.23
Neutrophils	39.27	42.96
Eosinophils	17.96	6.978
cDCs	12.22	7.96
pDCs	2.193	2.167

* Cell % = cell # of a cell type × 100/all the cell # in the condition

Cell %	KO	WT
EB Macrophages	0.098	11.84
Neutrophils	5.435	8.61
B cells	4.879	38.5
Macrophages	29.24	19.31
T cells	57.3	17.48
cDCs	2.227	2.994
pDCs	0.819	1.276

* Cell % = cell # of a cell type × 100/all the cell # in the condition

Figure 6. Single-cell RNAseq analysis reveals loss of splenic mouse and human EB macrophages in HMOX-1$^{-/-}$ HIS mice. Mouse and human CD45^{+} cells were purified by positive magnetic isolation from hHSC-engrafted HMOX-1$^{-/-}$ and HMOX-1$^{+/+}$ MSRG47 mice. Mouse and human CD45^{+} cells were individually analyzed by single-cell RNAseq and UMAPs shown for mouse CD45^{+} cells (A) and human CD45^{+} cells (B). Tables to the right of the UMAPs show changes in specific leukocyte subsets between HMOX-1$^{-/-}$ (KO) and HMOX-1$^{+/+}$ (WT). KO, knockout; UMAP, uniform manifold approximation and projection.

what has been observed in the MISTRG HIS model.[2,13,39] Because of the increased human macrophages, HIS models with humanized M-CSF have a high attrition rate, primarily believed to be due to anemia resulting from the murine RBCs being phagocytosed by human macrophages.[2] Although there are appreciable levels of hRBCs in the peripheral blood of HMOX-1$^{-/-}$ hSIRPα/hM-CSF/hCD47/Rag2$^{-/-}$/IL-2Rγ$^{-/-}$ HIS mice, these levels are insufficient to overcome the anemia resulting from the increased human macrophages. Thus, CD47, the ligand for SIRPα that triggers a "don't-eat-me signal," is also humanized to mitigate murine RBCs being engulfed by increased human macrophages,[40,41] increasing the survival of this HIS model. With the advent of a HIS model with hRBCs present in peripheral blood, the next challenge would be to increase hRBC output to overcome this anemia resulting from humanization of M-CSF. Such an HMOX-1$^{-/-}$ HIS model with humanized M-CSF would potentially not require humanized CD47 but would rather benefit from the loss of mouse RBCs and possibly their replacement with hRBCs.

HMOX-1$^{-/-}$ HIS mice have even higher levels of human myeloid cells and human CD36^{+}/CD206^{+} macrophages than HMOX-1$^{+/+}$ HIS mice. In the liver, this indicates that there is an increase in

human Kupffer cells. A possible explanation is that the loss of murine macrophages opens a cellular niche that enhances human macrophage development. Increased human NK cells are also observed in certain tissues, which is probably a result of elevated human myeloid cells that produce human IL-15, potentiating human NK cell development.[2,4]

Despite an overall increase in human macrophages, single-cell RNAseq analysis of the human immune compartment in HSC-engrafted HMOX-1$^{-/-}$ mice revealed that there was also a loss of specific human macrophage subsets that have a similar genetic signature (denoted by *EpoR* and *HMOX-1* genes) as the murine macrophage population lost in HMOX-1$^{-/-}$ mice. Upon the loss of murine erythrophagocytic cells, there is a subsequent dysregulation of the iron recycling pathway with oxidatively stressed RBCs that have an increased life span to compensate for the anemia resulting from this dysregulation.[27,42] However, it is possible that specific human erythrophagocytic macrophage subsets are engulfing oxidatively stressed mouse RBCs and the macrophages are being overloaded with toxic heme, which overwhelms the capacity of HMOX-1$^{+/+}$ human macrophages to manage. Furthermore, secondary byproducts may be produced in the blood of HMOX-1$^{-/-}$ mice (increased ferritin, bilirubin, etc) that may have deleterious effects on phagocytic human macrophages. Additional in vitro studies with HMOX-1$^{+/+}$ vs HMOX-1$^{-/-}$ mouse blood added to human macrophages could shed light on this loss of specific human EB macrophages. Even more surprising is the reduction in human B cells in the spleen of HSC-engrafted HMOX-1$^{-/-}$ mice. Loss of mouse B cells has not been reported in immune-competent HMOX-1$^{-/-}$ mouse models. Theoretically, soluble byproducts generated in HMOX-1$^{-/-}$ blood could be having a specific effect on human B cells in the peripheral tissues. Alternatively, HIS engraftment might be increased in HMOX-1$^{-/-}$ mice with increased myeloid/NK cells. It is possible that skewing toward myeloid/NK cells may be impacting human B-cell lymphopoiesis.

There is evidence that human macrophages in the HMOX-1$^{-/-}$ HIS mice are compensating for the loss of murine erythryophagocytic macrophages because of amelioration of certain pathologies associated with HMOX-1$^{-/-}$ mice.[23,26,29] Elevated heme levels in serum and spleen, as well as iron deposition in the kidneys of HMOX-1$^{-/-}$ mice, are decreased upon HIS engraftment. This suggests that human macrophages may be clearing excessive heme and iron upon HIS engraftment. Similarly, Kovtunovych et al[29] showed that BM transfer of WT mouse BM ameliorated pathology observed in HMOX-1–deficient mice. Nonengrafted HMOX-1$^{-/-}$ mice are comparable to nonengrafted HMOX-1$^{+/+}$ mice, as evidenced by the absence of any severe kidney or liver pathology and further corroborated by serum chemistry analyses. Indeed, HMOX-1$^{-/-}$ mice in an immune-deficient background appear to be healthier than those in an immune-competent background, for which severe kidney and liver pathology have been reported. Furthermore, because of pathologies, HMOX-1$^{-/-}$ mice have to be generated from HMOX-1$^{+/-}$ intercrosses,[23] whereas HMOX-1$^{-/-}$ mice in an MSRG47 background can be bred through HMOX-1$^{-/-}$ intercrosses. A benefit of this reduction in pathology is that it renders the HMOX-1$^{-/-}$ HIS mouse model more practical for experimental use and preclinical testing because of ease of breeding and longer life span.

Overall, a major advantage of the HMOX-1$^{-/-}$ HIS model is its potential for studying hematologic diseases that affect hRBCs such as sickle cell anemia and beta thalassemia.[13] hHSCs from patients with such hematologic diseases could be engrafted into HMOX-1$^{-/-}$ HIS mice, providing an in vivo model to test potential therapeutics.[13] A limitation that remains is that most RBCs are still murine; thus, hRBC output from the BM needs to be enhanced in the HMOX-1$^{-/-}$ HIS model. This low frequency limits the ability to study hEPO function in vivo because the primary purpose of RBCs to ferry oxygen is primarily carried out by the mouse RBCs. Human erythroblast reconstitution still remains relatively too low and variable to comprehensively assess function and ontogenetic development. Thus, to further potentiate the practicality of this mouse model, additional strategies are warranted to increase hRBC output given that HMOX-1 deficiency allows hRBC persistence in peripheral blood. Because hEPO can increase hRBCs in the peripheral blood of engrafted mice, humanization of EPO in this mouse model may potentiate hRBC levels.

In vivo models of malaria have been impeded by the lack of hRBCs in mouse models because malaria parasites specifically infect hRBCs.[17] An HIS mouse model that also has hRBCs can potentially be used to test human-specific immune-modulatory therapeutics in an in vivo malaria model.

Acknowledgments

The authors thank Mark Eckersdorff for his help in manuscript preparation, Hans Gartner for cloning the HMOX-1 deletion into the MSRG47 embryonic stem cells, and Melanie Buckman for help with mouse colony management.

Authorship

Contribution: A.K.P. and K.T. engrafted mice and performed experiments; H.K. and W.L. analyzed molecular profiling data; C.A. and B.P. prepared samples for single-cell RNA sequencing; M.N., Y.W., and G.S.A. provided guidance on molecular profiling of mouse and human samples; P.B. performed serum chemistry analysis; V.K. and D.A. analyzed histology; J.Z. managed mouse husbandry and establishment of the MSRG47 HMOX-1$^{-/-}$ mouse line; N.T. designed the HMOX-1 deletion to be cloned and targeted; L.M. and A.M. provided support and guidance on this project; and D.F. developed the idea of using HMOX-1–deficient mice for human red blood cell survival, led the project, and wrote the manuscript.

Conflict-of-interest disclosure: All authors are current or former employees of Regeneron Pharmaceuticals, Inc and may hold stock and/or stock options in the company. D.F. and N.T. are inventors on a US patent application no. 18/223,434 entitled "Genetically modified non-human animals and methods of use thereof."

ORCID profiles: K.T., 0000-0001-9161-0178; H.K., 0000-0003-0947-3149; W.L., 0000-0002-6226-2570; C.A., 0009-0005-2557-6246; B.P., 0000-0002-9938-9049; D.A., 0000-0001-5007-1163.

Correspondence: Davor Frleta, Regeneron Pharmaceuticals, Inc, 795 Old Saw Mill River Rd, Suite 92-106, Tarrytown, NY 10591; email: Davor.Frleta@regeneron.com.

References

1. Hu Z, Yang YG. Full reconstitution of human platelets in humanized mice after macrophage depletion. *Blood*. 2012;120(8):1713-1716.
2. Rongvaux A, Willinger T, Martinek J, et al. Development and function of human innate immune cells in a humanized mouse model. *Nat Biotechnol*. 2014; 32(4):364-372.
3. Yu H, Borsotti C, Schickel JN, et al. A novel humanized mouse model with significant improvement of class-switched, antigen-specific antibody production. *Blood*. 2017;129(8):959-969.
4. Herndler-Brandstetter D, Shan L, Yao Y, et al. Humanized mouse model supports development, function, and tissue residency of human natural killer cells. *Proc Natl Acad Sci U S A*. 2017;114(45):E9626-E9634.
5. Lee YS, O'Brien LJ, Walpole CM, et al. Human CD141(+) dendritic cells (cDC1) are impaired in patients with advanced melanoma but can be targeted to enhance anti-PD-1 in a humanized mouse model. *J Immunother Cancer*. 2021;9(3):e001963.
6. Ma SD, Xu X, Jones R, et al. PD-1/CTLA-4 blockade inhibits Epstein-Barr virus-induced lymphoma growth in a cord blood humanized-mouse model. *PLoS Pathog*. 2016;12(5):e1005642.
7. Wei J, Montalvo-Ortiz W, Yu L, et al. CD22-targeted CD28 bispecific antibody enhances antitumor efficacy of odronextamab in refractory diffuse large B cell lymphoma models. *Sci Transl Med*. 2022;14(670):eabn1082.
8. Wen J, Wang L, Ren J, et al. Nanoencapsulated rituximab mediates superior cellular immunity against metastatic B-cell lymphoma in a complement competent humanized mouse model. *J Immunother Cancer*. 2021;9(2):e001524.
9. Wong KK, Brenneman F, Chesney A, Spaner DE, Gorczynski RM. Soluble CD200 is critical to engraft chronic lymphocytic leukemia cells in immunocompromised mice. *Cancer Res*. 2012;72(19):4931-4943.
10. Garcia-Perez L, van Roon L, Schilham MW, Lankester AC, Pike-Overzet K, Staal FJT. Combining mobilizing agents with busulfan to reduce chemotherapy-based conditioning for hematopoietic stem cell transplantation. *Cells*. 2021;10(5):1077.
11. Zheng Y, Sefik E, Astle J, et al. Human neutrophil development and functionality are enabled in a humanized mouse model. *Proc Natl Acad Sci U S A*. 2022;119(43):e2121077119.
12. Coughlan AM, Harmon C, Whelan S, et al. Myeloid engraftment in humanized mice: impact of granulocyte-colony stimulating factor treatment and transgenic mouse strain. *Stem Cells Dev*. 2016;25(7):530-541.
13. Song Y, Shan L, Gbyli R, et al. Combined liver-cytokine humanization comes to the rescue of circulating human red blood cells. *Science*. 2021; 371(6533):1019-1025.
14. Little MA, Al-Ani B, Ren S, et al. Anti-proteinase 3 anti-neutrophil cytoplasm autoantibodies recapitulate systemic vasculitis in mice with a humanized immune system. *PLoS One*. 2012;7(1):e28626.
15. Brainard DM, Seung E, Frahm N, et al. Induction of robust cellular and humoral virus-specific adaptive immune responses in human immunodeficiency virus-infected humanized BLT mice. *J Virol*. 2009;83(14):7305-7321.
16. Hu Z, Van Rooijen N, Yang YG. Macrophages prevent human red blood cell reconstitution in immunodeficient mice. *Blood*. 2011;118(22):5938-5946.
17. Foquet L, Schafer C, Minkah NK, et al. Plasmodium falciparum liver stage infection and transition to stable blood stage infection in liver-humanized and blood-humanized FRGN KO mice enables testing of blood stage inhibitory antibodies (reticulocyte-binding protein homolog 5) in vivo. *Front Immunol*. 2018;9:524.
18. Yamaguchi T, Katano I, Otsuka I, et al. Generation of novel human red blood cell-bearing humanized mouse models based on C3-deficient NOG mice. *Front Immunol*. 2021;12:671648.
19. Dai XM, Ryan GR, Hapel AJ, et al. Targeted disruption of the mouse colony-stimulating factor 1 receptor gene results in osteopetrosis, mononuclear phagocyte deficiency, increased primitive progenitor cell frequencies, and reproductive defects. *Blood*. 2002;99(1):111-120.
20. Gyori DS, Mocsai A. Osteoclast signal transduction during bone metastasis formation. *Front Cell Dev Biol*. 2020;8:507.
21. Mun SH, Park PSU, Park-Min KH. The M-CSF receptor in osteoclasts and beyond. *Exp Mol Med*. 2020;52(8):1239-1254.
22. Keshvari S, Caruso M, Teakle N, et al. CSF1R-dependent macrophages control postnatal somatic growth and organ maturation. *PLoS Genet*. 2021; 17(6):e1009605.
23. Poss KD, Tonegawa S. Heme oxygenase 1 is required for mammalian iron reutilization. *Proc Natl Acad Sci U S A*. 1997;94(20):10919-10924.
24. Kawashima A, Oda Y, Yachie A, Koizumi S, Nakanishi I. Heme oxygenase-1 deficiency: the first autopsy case. *Hum Pathol*. 2002;33(1):125-130.
25. Yachie A, Niida Y, Wada T, et al. Oxidative stress causes enhanced endothelial cell injury in human heme oxygenase-1 deficiency. *J Clin Invest*. 1999; 103(1):129-135.
26. Kovtunovych G, Eckhaus MA, Ghosh MC, Ollivierre-Wilson H, Rouault TA. Dysfunction of the heme recycling system in heme oxygenase 1-deficient mice: effects on macrophage viability and tissue iron distribution. *Blood*. 2010;116(26):6054-6062.
27. Fraser ST, Midwinter RG, Coupland LA, et al. Heme oxygenase-1 deficiency alters erythroblastic island formation, steady-state erythropoiesis and red blood cell lifespan in mice. *Haematologica*. 2015;100(5):601-610.
28. Poss KD, Tonegawa S. Reduced stress defense in heme oxygenase 1-deficient cells. *Proc Natl Acad Sci U S A*. 1997;94(20):10925-10930.

29. Kovtunovych G, Ghosh MC, Ollivierre W, et al. Wild-type macrophages reverse disease in heme oxygenase 1-deficient mice. *Blood*. 2014;124(9):1522-1530.

30. Kim KS, Zhang DL, Kovtunovych G, et al. Infused wild-type macrophages reside and self-renew in the liver to rescue the hemolysis and anemia of Hmox1-deficient mice. *Blood Adv*. 2018;2(20):2732-2743.

31. Adamiak M, Moore JBt, Zhao J, et al. Downregulation of heme oxygenase 1 (HO-1) activity in hematopoietic cells enhances their engraftment after transplantation. *Cell Transplant*. 2016;25(7):1265-1276.

32. Malik J, Kim AR, Tyre KA, Cherukuri AR, Palis J. Erythropoietin critically regulates the terminal maturation of murine and human primitive erythroblasts. *Haematologica*. 2013;98(11):1778-1787.

33. Fouquet G, Thongsa-Ad U, Lefevre C, et al. Iron-loaded transferrin potentiates erythropoietin effects on erythroblast proliferation and survival: a novel role through transferrin receptors. *Exp Hematol*. 2021;99:12-2020.e3e3.

34. Manz MG. Human-hemato-lymphoid-system mice: opportunities and challenges. *Immunity*. 2007;26(5):537-541.

35. Romano L, Seu KG, Papoin J, et al. Erythroblastic islands foster granulopoiesis in parallel to terminal erythropoiesis. *Blood*. 2022;140(14):1621-1634.

36. Li W, Wang Y, Zhao H, et al. Identification and transcriptome analysis of erythroblastic island macrophages. *Blood*. 2019;134(5):480-491.

37. Li W, Guo R, Song Y, Jiang Z. Erythroblastic island macrophages shape normal erythropoiesis and drive associated disorders in erythroid hematopoietic diseases. *Front Cell Dev Biol*. 2020;8:613885.

38. An X, Mohandas N. Erythroblastic islands, terminal erythroid differentiation and reticulocyte maturation. *Int J Hematol*. 2011;93(2):139-143.

39. Rathinam C, Poueymirou WT, Rojas J, et al. Efficient differentiation and function of human macrophages in humanized CSF-1 mice. *Blood*. 2011;118(11):3119-3128.

40. Swoboda DM, Sallman DA. The promise of macrophage directed checkpoint inhibitors in myeloid malignancies. *Best Pract Res Clin Haematol*. 2020;33(4):101221.

41. Oronsky B, Carter C, Reid T, Brinkhaus F, Knox SJ. Just eat it: a review of CD47 and SIRP-alpha antagonism. *Semin Oncol*. 2020;47(2-3):117-124.

42. Cao YA, Kusy S, Luong R, Wong RJ, Stevenson DK, Contag CH. Heme oxygenase-1 deletion affects stress erythropoiesis. *PLoS One*. 2011;6(5):e20634.